A Practical Approach To Design Lattice Filters On Silicon Photonics

L. P. B. Lacerda[1,2]
leonardo.lacerda@ee.ufcg.edu.br
leonardopessoa@usp.br

Í. A. Araújo[1]
italo.araujo@ee.ufcg.edu.br

M. A. Romero[2]
murilo.romero@usp.br

A. F. Herbster[3]
adolfofh@dee.ufcg.edu.br

[1] *VIRTUS-CC*, Federal University of Campina Grande, Campina Grande, Paraíba, Brazil
[2] *Department of Electrical and Computer Engineering*, University of São Paulo - EESC/USP, São Carlos, São Paulo, Brazil
[3] *Department of Electrical Engineering*, Federal University of Campina Grande, Campina Grande, Paraíba, Brazil

***Abstract*—The design of higher-order optical filters often lacks a systematic and accessible synthesis procedure for practical implementation. This paper addresses this gap by presenting a general algorithm for synthesizing Nth-order 2x2 FIR half-band lattice filters using cascaded Mach-Zehnder Interferometers (MZIs). Implemented as a dedicated Python software tool, the method automates the computation of the required coupling and phase parameters. The effectiveness of the algorithm is confirmed through simulations of second- and third-order filters and experimentally with a fabricated fourth-order filter, which showed excellent agreement with the theoretical model. This work delivers a practical and efficient methodology for designing complex lattice filters, particularly for the silicon photonics platform.**

***Index Terms*—Lattice filters, Optical FIR filters, Mach-Zehnder Interferometer, Integrated photonics, Filter design, Intelligent Sensing.**

I. Introduction

The design of optical filters with well-defined and predictable spectral responses remains a key challenge in integrated photonics. Among the available architectures, 2×2 lattice-form filters based on cascaded Mach-Zehnder Interferometers (MZIs) offer a promising solution, due to their ability to produce flat-top and symmetric responses. However, despite their potential, most of the literature lacks accessible examples or practical synthesis procedures, especially for higher-order filters.

Several foundational works [1]–[4] present important theoretical frameworks for lattice-based optical circuits. Yet, the complexity of the algorithms and the absence of step-by-step demonstrations often limit their applicability. More recent studies focused on MZI-based filters [5], [6] achieve excellent performance but are typically tailored to specific use cases, lacking general design guidelines. These filters are particularly promising for applications in field-programmable photonic gate arrays (FPPGAs), which have emerged as flexible platforms for signal processing and filtering [7], [8].

This paper addresses these gaps by introducing a general and systematic algorithm for synthesizing 2×2 FIR lattice optical filters of arbitrary order for silicon photonics. The method directly yields the required coupling coefficients and phase shifts for each stage. To demonstrate the methodology, design examples for a second and third order filter are presented. The algorithm is then experimentally validated using a fabricated photonic chip with a fourth-order filter. The results confirm that this approach enables a reliable and reproducible design process, the analytical calculations have been implemented in a software tool [10], ensuring that the method is suitable for practical applications.

The paper is organized as follows. Section **I** presents the motivation and objectives of this study. Section **II** reviews the fundamentals of MZI and details the proposed recursive algorithm for lattice filter design. Section **III** defines the design procedure and illustrates the application of the algorithm through two practical examples. In Section **IV**, an ideal example of the filter is implemented. Section **V** discusses both the simulation and the experimental results obtained for the implemented filter. Finally, Section **VI** summarizes the main contributions and conclusions of this work.

II. Theory and Algorithm

A. Mach-Zehnder Interferometer

Lattice filters are recursive structures composed of cascaded stages, each defined by reflection and transmission coefficients. In the optical domain, each stage can be physically implemented using unbalanced MZIs, optical ring resonators (ORRs), or hybrid structures such as Ring-Assisted Mach-Zehnder Interferometer (RAMZI) filters. In this work, we focus on implementing lattice filters using MZIs as the fundamental filtering cells in silicon photonics. To model the effect of the differential delay introduced by the unbalanced arms, we define the delay matrix of the n-th stage as [1]:

$$S_d(z) = \begin{bmatrix} e^{j\phi_n} z^{-1} & 0 \\ 0 & 1 \end{bmatrix} \tag{1}$$

This work was supported in part by the PHOSENSE DEVICES project, supported by Centro De Competência EMBRAPII VIRTUS em Hardware Inteligente para Indústria - VIRTUS-CC, with financial resources from the PPI HardwareBR of the MCTI grant number 055/2023, signed with EMBRAPII, in part by the Conselho Nacional de Desenvolvimento Científico e Tecnologico (CNPq – 309343/2021-6) and in part by the Fundação de Amparo à Pesquisa do Estado de São Paulo (FAPESP – 2021/06569-1).

where the exponential term $e^{j\phi_n}$ represents the phase shift accumulated in the longer arm, and the discrete-time delay is modeled by z^{-1}. The phase shift ϕ_n is given by:

$$\phi_n = \frac{2\pi N_{eff} \Delta L}{\lambda} \tag{2}$$

where N_{eff} is the effective index of the waveguide, λ is the operating wavelength and ΔL the path length diference of the arms of the MZI.

The MZI also includes a power splitting component (usually a directional coupler), responsible for splitting and recombining the optical signal. This behavior is characterized by the through-port (c_n) and the cross-port (s_n) amplitude coefficients. These are related to the power coupling ratio, k_n, by the expressions $c_n = \sqrt{1-k_n}$ and $s_n = \sqrt{k_n}$. Its coupling matrix is given by:

$$S_c = \begin{bmatrix} c_n & -js_n \\ -js_n & c_n \end{bmatrix} \tag{3}$$

In this work, the parameter obtained by the step-down regression is the coupling angle θ, this represents the angle that generates the coupling coefficient k by the expression:

$$k = \sin^2(\theta) \tag{4}$$

Expanding the matrices, the complete transfer matrix becomes:

$$\begin{bmatrix} X_n(z) \\ Y_n(z) \end{bmatrix} = S_d(z) S_c(z) = \begin{bmatrix} c_n e^{j\phi_n} z^{-1} & -js_n \\ -js_n e^{j\phi_n} z^{-1} & c_n \end{bmatrix} \tag{5}$$

The recursive relation described above forms the basis for building lattice filters using cascaded MZIs, enabling the synthesis of complex spectral responses with tunable parameters. Fig. 1 shows a schematic of a second-order lattice filter. In this architecture, the parameters θ_0, θ_1, and θ_2 represent the coupling angles of the successive MZI stages, while φ_1 and φ_2 are the differential phase shifts applied in the corresponding interferometer arms. Based on this principle, the theoretical framework provides a practical guide for designing such filters, linking the physical structure of the device to the desired frequency response and supporting a simplified algorithm for determining the coupling parameters at each stage.

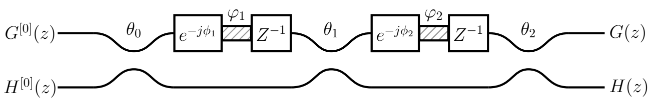

Fig. 1: Example of a second order Lattice Filter using cascaded MZIs.

B. Properties and Characteristics

This work models the device as a lossless 2×2 optical filter, whose bar ($G(z)$) and cross ($H(z)$) transfer functions must satisfy the power conservation condition $G(z)G^*(z) + H(z)H^*(z) = I$ [2]. The filters are specifically designed to adhere to the half-band property, which imposes a spectral symmetry defined in the z-domain:

$$F(z)F^*(z) + F(-z)F^*(-z) = 1, \tag{6}$$

where $F(z)$ represents the filter response and $F^*(z)$ is its para-Hermitian conjugate. This property is physically realized using a circuit of N cascaded MZIs, where, following the configuration in [2], $N-1$ stages have a path length difference of $2\Delta L$ while one stage has a fundamental difference of ΔL. This fundamental path length difference, ΔL, ultimately sets the filter's Free Spectral Range (FSR) according to:

$$\text{FSR} \approx \frac{\lambda_0^2}{n_g \Delta L}. \tag{7}$$

C. Definitions for Design

Let the matrix representation of the $N-1$ MZIs with a path length difference of $2\Delta L$ be defined as:

$$S^{[n]}(z) = \begin{pmatrix} G^{[n]}(z) & jH^{*[n]}(z) z^{-2(N-1)} \\ jH^{[n]}(z) & G^{*[n]}(z) z^{-2(N-1)} \end{pmatrix} \tag{8}$$

where $G^{[n]}(z)$ and $H^{[n]}(z)$ denote the bar and cross transfer functions for the n-th stage, respectively. It is important to note that this configuration is restricted to the implementation of only odd-order half-band filters. The power transmission characteristics of FIR half-band filters can be expressed as

$$G(z)G_*(z) = \frac{1}{2}\left(\sum_{k=1}^{N} A_{2k-1} z^{-(2k-1)} + \sum_{k=1}^{N} A^*_{2k-1} z^{2k-1} \right) \tag{9}$$

$$H(z)H_*(z) = \frac{1}{2}\left(-\sum_{k=1}^{N} A_{2k-1} z^{-(2k-1)} + \sum_{k=1}^{N} A^*_{2k-1} z^{2k-1} \right) \tag{10}$$

where the coefficients satisfy $A_{2k-1} = A^*_{-(2k-1)}$, ensuring para-Hermitian symmetry, i.e., [2]. These expressions assume that the coefficients A_{2k-1}, with $k = 1, \ldots, N$, are selected to match a desired power transmission spectrum.

The power coefficients A are determined by the desired symmetric filter specifications. In the example presented in this work, reference [9] provides weighting coefficients for certain maximally flat non-recursive digital filters. In this case, the weights w_i are applied only to the odd-order polynomial terms, where $i = 2N-1$, while the even-order terms are assigned zero.

III. Design Procedure and Application

The flowchart in Fig. 2 defines the steps from the creation of the polynomial to the coupling coefficients of the lattice filter.

The first step is to select the polynomial power coefficients, $\{A_k\}$, for the target filter order. Then, associated with the given spectral profile, the power transfer functions $G(z)G_*(z)$ and $H(z)H_*(z)$ are calculated (Eq. (9) and Eq. (10)) and the zeros of the polynomials are computed and organized into conjugate reciprocal pairs $(\alpha_n, 1/\alpha_n^*)$.

Once the zero sets $\{\alpha_k\}$ are defined, the transfer functions $G(z)$ and $H(z)$ are calculated as:

$$G(z) = a_0 \prod_{k=1}^{2N-1} \left(1 - \alpha_k z^{-1}\right), \tag{11}$$

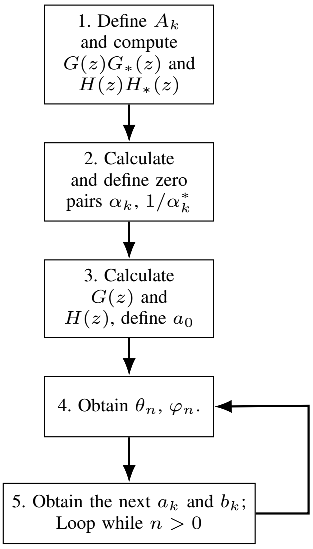

Fig. 2: Block diagram for the purposed algorithm.

$$H(z) = a_0 \prod_{k=1}^{2N-1} \left(1 + \alpha_k z^{-1}\right), \tag{12}$$

where the scalar a_0 ensures the lossless condition. With $G(z)$ and $H(z)$ defined, the stepdown decomposition procedure is used to iteratively extract the coupling coefficients (θ_n, φ_n) for each MZI stage in the lattice:

$$\theta_n = \tan^{-1}\left(b_n^{[n]}/a_n^{[n]}\right), \tag{13}$$

$$\varphi_n = -\arg\left(\frac{a_1^{[n]} b_0^{[n]} - a_0^{[n]} b_1^{[n]}}{(a_0^{[n]})^2 + (b_0^{[n]})^2}\right). \tag{14}$$

Finally, the expansion coefficients must be updated using the following recurrence relations:

$$\begin{cases} a_k^{[n-1]} &= (a_k^{[n]} \cos\theta_n - b_k^{[n]} \sin\theta_n) e^{j\frac{\varphi_n}{2}} \\ b_k^{[n-1]} &= (a_{k+1}^{[n]} \sin\theta_n + b_{k+1}^{[n]} \cos\theta_n) e^{-j\frac{\varphi_n}{2}} \end{cases} \tag{15}$$

with $(k = 0, 1, \ldots, n-1)$. The procedure follows a coefficient ordering convention from highest (index 0) to lowest (index n).

A. Application

1) Second Order Filter: For a second-order symmetric maximally flat filter, the power coefficients A_k obtained from [9] are defined as $A_0 = 0.5$, $A_1 = 0.28125$, $A_2 = 0$, and $A_3 = 0.03125$. Defining $FSR = 25\ nm$, $L = 50\ \mu m$, $n_g = 4.2$, $N_{eff} = 2.44$, $\lambda_0 = 1550\ nm$, Eq. (7) give us $\Delta L = 22.88\ \mu m$. By applying Eq. (9) and (10), we obtain:

$$G(z)G_*(z) = 1/2 + \left(A_1 z^{-1} + A_3 z^{-3}\right) + \left(A_{-1} z + A_{-3} z^3\right) \tag{16}$$

$$H(z)H_*(z) = 1/2 + \left(A_1 z^{-1} + A_3 z^{-3}\right) + \left(A_{-1} z + A_{-3} z^3\right) \tag{17}$$

Given the roots of $G(z)$, $\alpha_1 = -0.26795$, $\alpha_2 = 0.99989 + 0.0011j$, $\alpha_3 = 0.99989 - 0.00011j$ and $a_0 = 0.3415$:

$$G(z) = -0.3415 - 0.59151 z^{-1} - 0.15850 z^{-2} + 0.09151 z^{-3} \tag{18}$$

$$H(z) = 0.3415 - 0.59151 z^{-1} + 0.15850 z^{-2} + 0.09151 z^{-3} \tag{19}$$

TABLE I: Polynomial coefficients for $n = 2$ of $G(z)$ and $H(z)$ mapped to a_k and b_k

$G(z)$ **Coefficient** (a_k)	$H(z)$ **Coefficient** (b_k)
$a_0 = +0.09151$	$b_0 = +0.09151$
$a_1 = -0.15850$	$b_1 = +0.15850$
$a_2 = -0.59151$	$b_2 = -0.59151$
$a_3 = -0.3415$	$b_3 = +0.3415$

With the coefficients a_n and b_n determined, shown in Table I, and using Eq. (11), we compute the filter filter parameters θ_2 and φ_2:

$$\theta_2 = \left|\tan^{-1}\left(\frac{b_2^{[2]}}{a_2^{[2]}}\right)\right| \approx -\frac{\pi}{4} \tag{20}$$

$$\varphi_2 = -\arg\left(\frac{a_1^{[2]} b_0^{[2]} - a_0^{[2]} b_1^{[2]}}{(a_0^{[2]})^2 + (b_0^{[2]})^2}\right) = -\pi \tag{21}$$

Subsequently, the next set of a_k and b_k coefficients are obtained from Eq. (15), shown in Table II:

TABLE II: Polynomial coefficients for $n = 1$ of $G^{[1]}(z)$ and $H^{[1]}(z)$ mapped to a_k and b_k

$G^{[1]}(z)$ **Coefficient** (a_k)	$H^{[1]}(z)$ **Coefficient** (b_k)
$a_0 = 0. - 0.1294j$	$b_0 = 0. + 0.22409j$
$a_1 = -0. + 0.8365j$	$b_1 = 0. + 0.48302j$

Thus, the coupling and phase parameters for this step-down stage are $\theta_1 \approx -\pi/3$, $\varphi_1 = 0$.

Finally, for the last coupling angle, we use the same method as previous, resulting on:

$$a_0^{[0]} = 0. + 0.12936j; \quad b_0^{[0]} = 0. - 0.48288j; \tag{22}$$

thus $\theta_0 =\approx -0.4167\pi$:

TABLE III: Coupling and phase parameters for each stage of the second-order filter

Stage	**Coupling Angle** θ_n	**Coupling Coef.** k_n	**Phase** φ_n
$n = 2$	$\theta_2 = -\pi/4$	$k_2 = 0.5000$	$\varphi_2 = -\pi$
$n = 1$	$\theta_1 = -\pi/3$	$k_1 = 0.7500$	$\varphi_1 = 0$
$n = 0$	$\theta_0 \approx -0.4167\pi$	$k_0 = 0.9330$	—

The recursive application of the step-down algorithm enabled the extraction of all coupling and phase parameters required for the physical implementation of the second-order filter, as presented on Table III. This parameters can be directly implemented as shown on Fig.1

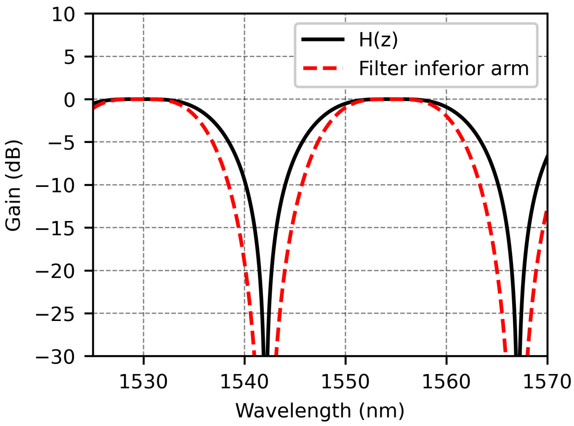

Fig. 3: Comparison between the simulated gain of the synthesized filter (red dashed line) and the target gain defined by the polynomial spectral response (black solid line) for the second-order filter.

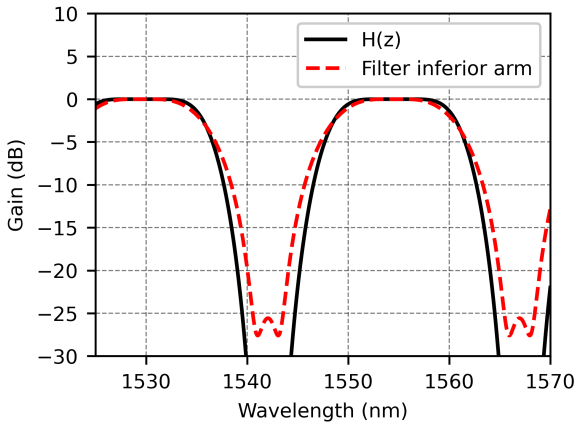

Fig. 4: Comparison between the simulated gain of the synthesized filter (red dashed line) and the target gain defined by the polynomial spectral response (black solid line) for the third-order filter.

2) Third-Order Filter: Similarly to the second-order case, a third-order filter is designed. The algorithm uses the coefficients $A_0 = 0.5$, $A_1 = -0.29297$, $A_2 = 0$, $A_3 = 0.04883$, $A_4 = 0$, and $A_5 = -0.00586$. This results in the following five polynomial roots: $\alpha_1 = -1.0021 + 0.j$, $\alpha_2 = -1.0011 - 0.00189j$, $\alpha_3 = -1.0011 + 0.00189j$, $\alpha_4 = -0.99891 - 0.00188j$, and $\alpha_5 = -0.99891 + 0.00188j$.

Applying the same algorithmic steps from the previous section yields the intermediate reflection coefficient $a_0 = 0.31216$. The final coupling angles (θ_n) and phase shifts (φ_n) required for each lattice stage are summarized in Table IV.

TABLE IV: Coupling and phase parameters for each stage of the third-order filter.

Stage	Coupling Angle	Coupling Coef. k_n	Phase Shift φ_n
$n = 3$	$\theta_3 = -\pi/4$	$k_3 = 0.5000$	$\varphi_3 = 0$
$n = 2$	$\theta_2 = -0.2499\pi$	$k_2 = 0.4998$	$\varphi_2 = 0$
$n = 1$	$\theta_1 = -0.4372\pi$	$k_1 = 0.9616$	$\varphi_1 = 0$
$n = 0$	$\theta_0 = -0.0461\pi$	$k0 = 0.0209$	—

IV. Simulations

To further validate the proposed algorithm, we simulated the second- and third-order lattice filters in an ideal scenario using the Lumerical INTERCONNECT platform. The filters were configured with the coupling coefficients and phase shifts derived from our synthesis process. The simulated transmission spectra were then compared to the theoretical responses of the target polynomials to assess the intrinsic accuracy provided by the algorithm.

The simulation results presented in Figs. 3 and 4 confirm the effectiveness of the proposed algorithm. The synthesized filters closely approximate the target spectral responses, albeit with some inherent artifacts from the synthesis method. The most notable deviation is a minor sidelobe in the stopband of the third-order filter (Fig. 4). This sidelobe is a predictable consequence of the zero-placement technique used to shape the filter response. In any case, the results demonstrate that the algorithm provides a quite satisfactory translation from a theoretical model to a physically realizable optical filter.

V. Results

To validate the proposed algorithm and associated simulations, a fourth-order lattice filter was fabricated using the parameters obtained from the synthesis process for $N = 4$. The chip was designed on a SOI (Silicon-On-Insulator) platform and fabricated through Electron Beam Lithography at Nanotools, using components from the EBeam library available via the SiEPIC EBL 2025-2 process. The estimated Free Spectral Range (FSR) was 20 nm, corresponding to a path length difference of $\Delta L \approx 28.5$ μm. The center wavelength was set to 1550 nm, with a waveguide width of 500 nm and height of 220 nm. The total chip area was 605×410 μm^2. An image of the fabricated chip is shown in Fig. 5.

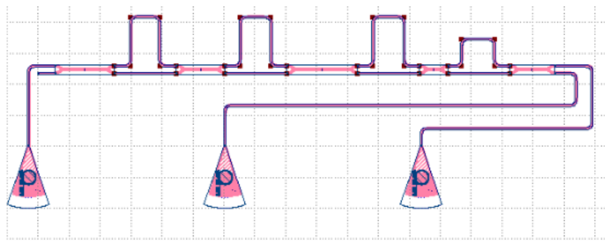

Fig. 5: Fabricated fourth-order lattice filter implemented with cascaded MZI structure.

Figures 6 and 7 present the measured transmission spectra for the superior and inferior arms of the filter, respectively, compared with the simulated responses obtained from the theoretical model.

The experimental data shows satisfactory agreement with the theoretical predictions, confirming the accuracy of the proposed synthesis method. Some discrepancies are observed in the form of elevated side-lobes and increased ripple in the measured spectra. These deviations are primarily attributed to

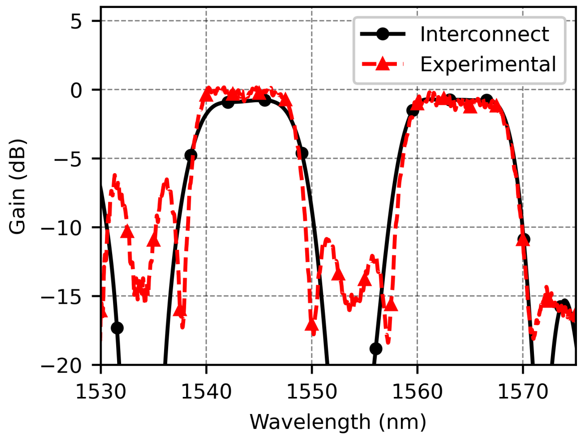

Fig. 6: Experimental results for the upper output: measured (red dashed line) vs. simulated (black solid line) transmission spectrum.

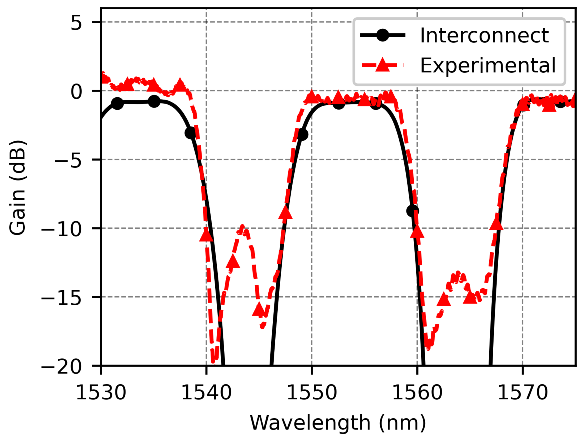

Fig. 7: Experimental results for the lower output: measured (red dashed line) vs. simulated (black solid line) transmission spectrum.

the high sensitivity of the directional couplers used in the design, which can lead to imbalance and unwanted perturbations in the filter's transfer function. Additionally, certain points in the measured spectrum exceed the maximum transmission level. This is due to the normalization being based on a reference straight waveguide, and can occur as a result of imperfections or losses in the reference path.

Overall, the results confirm the feasibility and effectiveness of the proposed algorithm for designing and implementing maximally flat optical lattice filters using cascaded MZI architectures.

VI. Conclusion

This paper presented a general and systematic algorithm for synthesizing Nth-order 2×2 lattice filters based on cascaded Mach-Zehnder Interferometer (MZI) structures. To make this method practical and reproducible, the algorithm was implemented in a Python-based software tool, in such way to automates the direct computation of all required coupling coefficients and phase shifts from a target spectral response using a recursive step-down approach.

The algorithm's performance was validated through both simulation and experimental results. Ideal simulations of second- and third-order filters confirmed that the method accurately reproduces the target spectral response. Next, a fourth-order filter was fabricated and tested. The experimental measurements showed excellent agreement with the theoretical model, validating the design process reliability even with predictable deviations caused by fabrication tolerance.

In conclusion, this work successfully contributes to bridge the gap between complex filter theory and practical implementation by providing a validated, software-enabled design methodology. The combination of a robust algorithm and an accessible software tool offers a powerful and efficient pathway to design and realize custom optical filters for advanced applications in integrated photonics.

References

[1] K. Jinguji, Y. Hida, M. Kawachi, "Synthesis of coherent two-port lattice-form optical delay-line circuit," *J. Lightwave Technol.*, vol. 13, no. 1, pp. 73–82, Jan. 1995.

[2] K. Jinguji, M. Oguma, "Optical half-band filters using lattice-form waveguide circuits," *J. Lightwave Technol.*, vol. 18, no. 2, pp. 252–259, Feb. 2000.

[3] A. Ananda, "Design and simulation of non-zero and zero dispersion optical lattice wavelength filters," Univ. Twente, 2004.

[4] J. D. Domenech and J. Capmany, "Optical filter design and analysis," in *Integrated Photonics*, UPV Press, Valencia, Spain, 2013, pp. 141–178.

[5] J. Horst et al., "Cascaded Mach–Zehnder wavelength filters," *Opt. Express*, vol. 21, no. 10, pp. 11652–11660, May 2013.

[6] Y. Xu et al., "Flat-top CWDM de-multiplexer based on cascaded MZIs," *IEEE Photon. Technol. Lett.*, vol. 30, no. 4, pp. 335–338, Feb. 2018.

[7] D. Pérez, I. Gasulla, and J. Capmany, "Compact programmable RF-photonic filters using integrated waveguide mesh processors," *Nat. Commun.*, vol. 8, no. 636, pp. 1–9, Sep. 2017.

[8] D. Pérez-López, A. Gutierrez, D. Sánchez *et al.*, "General-purpose programmable photonic processor for advanced radiofrequency applications," *Nat. Commun.*, vol. 15, no. 1563, pp. 1–9, Mar. 2024.

[9] C. Gumacos, "Weighting coefficients for certain maximally flat nonrecursive digital filters," *IEEE Trans. Circuits Syst.*, vol. CAS-25, no. 4, pp. 234–235, Apr. 1978.

[10] L. P. B. Lacerda, "Lattice-Filter-Synthesis-Tool," v1.0.0, 2025. [Online]. Available: https://github.com/Leoopessoa/Lattice-Filter-Synthesis-Tool. [Accessed: Jul. 3, 2025].